Supporting Information

Multicolor Photoluminescence of Cu_{14} Cluster Modulated by Surface Ligands

Arijit Jana[a], Subrata Duary[a], Amitabha Das[b], Amoghavarsha Ramachandra Kini[a], Swetashree Acharya[a], Jan Machacek[c], Biswarup Pathak[b]*, Tomas Base[c]* and Thalappil Pradeep[a]*

[a]DST Unit of Nanoscience (DST UNS) and Thematic Unit of Excellence (TUE), Department of Chemistry, Indian Institute of Technology, Madras, Chennai – 600036, India

[b]Department of Chemistry, Indian Institute of Technology Indore, Indore 453552, India

[c]Department of Syntheses, Institute of Inorganic Chemistry, The Czech Academy of Sciences, 1001 Husinec – Rez, 25068, Czech Republic

* pradeep@iitm.ac.in, tbase@iic.acs.cz, biswarup@iiti.ac.in

Table of content

Instrumentation

a) UV-vis absorption spectroscopy

UV-vis absorption spectra were measured in the wavelength range of 1100-200 nm using Perkin Elmer Lambda 365 UV-vis spectrometer, equipped with a bandpass filter of 1 nm. The scan rate of spectral acquisition is 100 nm/min.

b) Mass spectrometry

Mass spectra of the clusters were measured by Waters Synapt G2Si HDMS instrument. The instrument is equipped with a nano-electrospray ionization source, mass selected ion trap, ion mobility cells, and time of flight mass analyzer. Optimized operating conditions such as flow rate 10-15 μL/min, capillary voltage 2-3 kV, cone voltage 20 V, source offset 10 V, desolvation gas flow 400 L/min, source temperature 100 °C and desolvation temperature 150 °C were used for the measurements. Collision-induced dissociation (CID) studies were performed upon colliding the selected molecular ion with argon gas inside the trap cell of the instrument. Gradually increasing the collision energy (CE 0 to 200 for Cu_{14} and CE 0 to 100 for Cu_{14}-DMF) leads to the fragmentation of the species. All the measurements used low concentrations (~ 1 μg/ml) of cluster samples.

c) Photoluminescence spectroscopy

Photoluminescence spectra were measured using Horiba Jobin Yvon Nanolog spectrometers by applying 3 nm bandpass filter having a resolution bandwidth of 5 nm. The Nanolog instrument has a 450 W Xenon-arc lamp source, double monochromator with gratings, associated reflective optics, and CCD detector. Samples dissolved in the respective solvents were placed inside the 1 cm quartz cuvette to measure the spectrum.

Calculation of the relative quantum yield

We used our previously synthesized Cu_4-ICBT cluster (which has an emission maximum at 595 nm with an absolute quantum yield (QY) of 18% at room temperature) as a standard.[1] The relative quantum yield (RQY) of these Cu_{14} clusters was calculated using the following equation.

RQY-sample = QY-std * Exc.-std * Area (PL-sample) / Exc.-sample * Area (PL-std)

RQY Cu_{14}-solid = 10.04 ± 2.1 %; RQY Cu_{14}-DMF solid = 23.14 ± 1.5 %

RQY Cu_{14}-solution = 4.6 ± 1.2 %; RQY Cu_{14}-DMF solution = 15.05 ± 2.0 %

RQY Cu_{14}-fiber (green) = 39.23 ± 1.3 %; RQY Cu_{14}-fiber (yellow) = 41.71 ± 1.1 %

d) Optical microscopy

Optical microscopic images in transmission mode were collected using a LEICA optical microscope equipped with LAS V4.8 software. Polarization of the crystals were checked using an optical polarizer.

e) Scanning electron microscope

Scanning electron microscopic (SEM) images are recorded using a Verios G4 UC, Thermo Scientific field emission scanning electron microscope (FESEM). After transferring the sample on the carbon tape, gold sputtering was performed to increase the conductivity of the sample. All the FESEM images were collected in high vacuum at an operating voltage of 10-15 kV. Energy dispersive analysis of X-ray (EDAX) was performed using the same instrument.

f) Infrared spectroscopy

FT-IR spectra were measured in the transmission mode using a JASCO-4100 FT-IR spectrometer after preparing potassium bromide (KBr) pellets of the respective samples.

g) X-ray photoelectron spectroscopy

X-ray photoelectron spectroscopy (XPS) was performed using an Omicron Nanotechnology ESCA probe TPD spectrometer, equipped with polychromatic dual Mg Kα (hυ = 1253.6 eV) and Al Kα (hυ = 1486.6 eV) X-ray source. Clusters were drop casted onto the XPS grid for the measurements. Binding energy of the spectral regions of different elements were calibrated with respect to C 1s (285.0 eV).

h) Thermogravimetric analysis

Thermogravimetric measurements in the temperature range of 25 to 800 °C were measured using a NETZSCH STA 449 F3 Jupiter instrument equipped with Proteus-6.1.0 software. About 3-4 mg of crystalline sample was loaded in an alumina crucible for the measurement. Nitrogen and argon were used as protective environments. Thermal flow rate of the measurement was 10 °C/min.

i) TCSPC measurement

Time resolved PL lifetime measurements were performed using Horiba DeltaFlex time-correlated single photon count (TCSPC) spectrometer equipped with Horiba Delta diode 405 nm laser. Resulted emissive photons were collected using Horiba PPD-850 detector. The triexponential fittings of the decay curve was performed by deconvolution procedure of DAS6 (v. 6.8, Horiba Jobin Yvon) software.

j) Single crystal X-ray diffraction

Single crystal X-ray diffraction (SC-XRD) data collection was performed with Bruker D8 VENTURE single crystal X-ray diffractometer equipped with monochromatic Mo Kα (λ =

0.71073 Å) or Cu Kα (λ = 1.54178 Å) radiations and PHOTON 100 CMOS detector. The data collection was performed at 200-296 K based on the requirement of the specific crystals. The automatic cell determination routine, with 24 frames at two different orientations of the detector was employed to collect reflections for unit cell determination. Further, intensity data for structure determination were collected through an optimized strategy which gave an average 4-fold redundancy. The program APEX3-SAINT (Bruker, 2016) was used for integrating the frames, followed by a multi-scan absorption correction using the program SADABS (Bruker, 2016). The structure was solved by SHELXT-2014 (Sheldrick, 2014) and refined by full-matrix least squares techniques using SHELXL-2018, (Sheldrick, 2018) software package. Hydrogens on all carbon and boron atoms were fixed at calculated positions and refined by rigid body constrains with C-H or B-H = 1.10 Å. Sometimes different restraints (DFIX, SIMU, ISOR, DELU, etc.) were applied to their bond distances and thermal parameters (Uij) values during refinement to maintain sensible molecular geometry as well as reasonable anisotropic displacement parameter (ADP) values. Moreover, FLAT restraint was needed to be applied for atoms in the phenyl ring to lie in a common plane.

k) Powder X-ray diffraction

Powder XRD measurements were performed using a D8 Advance Bruker, using Cu Kα as the X-ray source (25 kV). Thin samples of clusters were placed on a clean glass slide for measurements.

l) Computational details

Molecular level Density Functional Theory (DFT) calculations were conducted using the Gaussian 09 D.01 program.[2] The Becke's three-parameter hybrid exchange functional and Lee-Yang-Parr's (B3LYP) correlation functional were implemented in conjunction with the Pople's 6-31G* basis set for non-metal elements and LANL2DZ-ECP (effective core potential) for Cu atoms.[3-6] For the TD-DFT calculations, 500 singlet-to-singlet excitation energies were considered. Structural optimization was performed for the S_0 and S_1 states of both the clusters. The wavefunction for the hole and electron pair distribution analysis of clusters were calculated using the UB3LYP functional. The Kohn-Sham orbital analysis and hole and electron pair distribution analysis were performed using Multiwfn.[7]

Table S1. Crystal data and structure refinement for Cu_{14}-DMF cluster

Identification code	Arijit-Cu_{14}	
Empirical formula	C30 H102 B60 Cu14 N6 O8 S12	
Formula weight	2598.05	
Temperature	297(2) K	
Wavelength	0.71073 Å	
Crystal system	Trigonal	
Space group	R -3:H	
Unit cell dimensions	a = 19.5323(4) Å	α= 90°
	b = 19.5323(4) Å	β= 90°
	c = 29.2601(6) Å	γ = 120°
Volume	9667.5(4) $Å^3$	
Z	3	
Density (calculated)	1.339 mg/m^3	
Absorption coefficient	2.485 mm^{-1}	
F(000)	3858	
Crystal size	0.260 x 0.250 x 0.200 mm^3	
Theta range for data collection	3.262 to 25.000°	
Index ranges	-23<=h<=23, -23<=k<=23, -34<=l<=34	
Reflections collected	48536	
Independent reflections	3786 [R(int) = 0.1415]	
Completeness to theta = 25.000°	99.6 %	
Absorption correction	Semi-empirical from equivalents	
Max. and min. transmission	0.4708 and 0.1730	
Refinement method	Full-matrix least-squares on F^2	
Data / restraints / parameters	3786 / 219 / 242	
Goodness-of-fit on F^2	1.040	
Final R indices [I>2sigma(I)]	R1 = 0.0560, wR2 = 0.1588	
R indices (all data)	R1 = 0.0850, wR2 = 0.1835	
Extinction coefficient	n/a	
Largest diff. peak and hole	1.028 and -0.657 $e.Å^{-3}$	

Table S2. Atomic coordinates (x 10^4) and equivalent isotropic displacement parameters ($Å^2$x 10^3) for Cu_{14}-DMF cluster. U(eq) is defined as one third of the trace of the orthogonalized U^{ij} tensor.

	x	y	z	U(eq)
Cu(1)	4841(1)	2431(1)	7961(1)	51(1)
Cu(2)	6229(1)	3797(1)	7959(1)	43(1)
Cu(3)	6667	3333	7174(1)	57(1)
O(1)	6667	3333	6390(4)	133(4)
O(2)	3542(14)	1600(20)	7655(14)	276(10)
N(1)	2367(17)	1460(20)	7526(14)	237(9)
C(3)	2798(19)	1110(20)	7738(17)	261(9)
C(4)	2530(30)	2200(20)	7743(17)	272(16)
C(5)	1512(19)	900(30)	7466(17)	241(15)
N(1')	2437(15)	1279(19)	7420(11)	230(8)
O(2')	3547(12)	2080(20)	7701(11)	298(10)
C(3')	2807(16)	1860(20)	7802(11)	250(9)
C(4')	3025(19)	1460(20)	7066(10)	234(12)
C(5')	1653(15)	1030(20)	7309(12)	233(12)
C(1)	5050(4)	5584(4)	7002(2)	66(2)
B(3)	5077(4)	5351(4)	7568(3)	59(2)
S(1)	5424(1)	3206(1)	7321(1)	45(1)
S(2)	6361(1)	5057(1)	8073(1)	44(1)
B(10)	5290(4)	4078(4)	7216(2)	48(2)
B(7)	4667(4)	4300(4)	7568(3)	51(2)
B(8)	5731(4)	4949(4)	7567(2)	47(2)
B(2)	5946(5)	5784(4)	7209(3)	59(2)
B(9)	6085(4)	5003(4)	6996(2)	53(2)
B(1)	5645(5)	5418(5)	6641(3)	73(2)
C(2)	4637(4)	4782(4)	6688(2)	67(2)
B(4)	4253(5)	4731(5)	7216(3)	73(2)
B(6)	4374(4)	3949(5)	6997(3)	58(2)
B(5)	5243(5)	4385(5)	6644(3)	58(2)

Table S3. Anisotropic displacement parameters ($Å^2 x\ 10^3$) for Cu_{14}-DMF cluster. The anisotropic displacement factor exponent takes the form: $-2\pi^2[h^2a^{*2}U^{11} + ... + 2\ h\ k\ a^*\ b^*\ U^{12}\ ]$

	U^{11}	U^{22}	U^{33}	U^{23}	U^{13}	U^{12}
Cu(1)	51(1)	53(1)	51(1)	1(1)	2(1)	27(1)
Cu(2)	46(1)	43(1)	44(1)	-2(1)	-5(1)	23(1)
Cu(3)	54(1)	54(1)	63(1)	0	0	27(1)
O(1)	153(7)	153(7)	93(8)	0	0	76(3)
O(2)	279(12)	253(13)	278(12)	-26(11)	-20(11)	121(10)
N(1)	246(12)	237(12)	241(12)	-4(10)	-48(10)	130(10)
C(3)	266(12)	253(12)	266(12)	-15(10)	-21(10)	131(9)
C(4)	280(20)	260(20)	260(20)	13(19)	-44(19)	114(18)
C(5)	270(20)	220(20)	170(20)	3(18)	-114(17)	72(17)
N(1')	242(11)	236(11)	239(12)	-9(10)	-46(10)	140(9)
O(2')	296(13)	278(13)	290(12)	-10(11)	-23(11)	122(10)
C(3')	255(11)	247(12)	260(11)	-10(10)	-27(10)	134(9)
C(4')	255(19)	221(18)	250(20)	4(17)	-47(17)	137(15)
C(5')	279(19)	178(17)	160(18)	4(15)	-145(15)	53(15)
C(1)	72(4)	65(4)	73(5)	9(4)	-13(4)	41(4)
B(3)	61(4)	55(4)	67(5)	2(4)	-6(4)	34(4)
S(1)	47(1)	44(1)	43(1)	-2(1)	-3(1)	23(1)
S(2)	45(1)	43(1)	43(1)	0(1)	-1(1)	22(1)
B(10)	45(4)	46(4)	51(4)	3(3)	-2(3)	22(3)
B(7)	48(4)	53(4)	54(4)	0(3)	-6(3)	27(3)
B(8)	51(4)	45(4)	49(4)	3(3)	-4(3)	27(3)
B(2)	58(4)	52(4)	63(5)	8(4)	-7(4)	25(4)
B(9)	55(4)	49(4)	53(4)	10(3)	-3(3)	24(3)
B(1)	82(6)	69(5)	65(5)	17(4)	-3(4)	36(5)
C(2)	73(4)	66(4)	64(4)	5(3)	-15(4)	37(4)
B(4)	66(5)	84(6)	85(6)	3(5)	-12(4)	49(5)
B(6)	52(4)	55(4)	65(5)	4(4)	-9(4)	26(4)
B(5)	65(5)	62(5)	48(4)	3(3)	-8(3)	33(4)

Table S4. Hydrogen coordinates (x 10^4) and isotropic displacement parameters ($Å^2$x 10^3) for the Cu_{14}-DMF cluster.

	x	y	z	U(eq)
H(3)	2586	637	7900	313
H(4A)	2235	2405	7591	408
H(4B)	2381	2108	8059	408
H(4C)	3086	2577	7720	408
H(5A)	1272	1177	7325	361
H(5B)	1435	472	7275	361
H(5C)	1272	706	7759	361
H(3')	2588	2008	8035	300
H(4'1)	3528	1617	7206	350
H(4'2)	2870	994	6883	350
H(4'3)	3064	1876	6877	350
H(5'1)	1353	941	7585	349
H(5'2)	1630	1430	7130	349
H(5'3)	1435	548	7137	349
H(1)	4968	6089	6924	80
H(2)	5021	5670	7862	70
H(2A)	4350	3937	7866	62
H(4)	6443	6381	7275	71
H(5)	6678	5093	6928	64
H(6)	5943	5774	6337	87
H(7)	4263	4733	6394	80
H(8)	3665	4656	7282	88
H(9)	3866	3362	6921	69
H(10)	5291	4077	6341	69

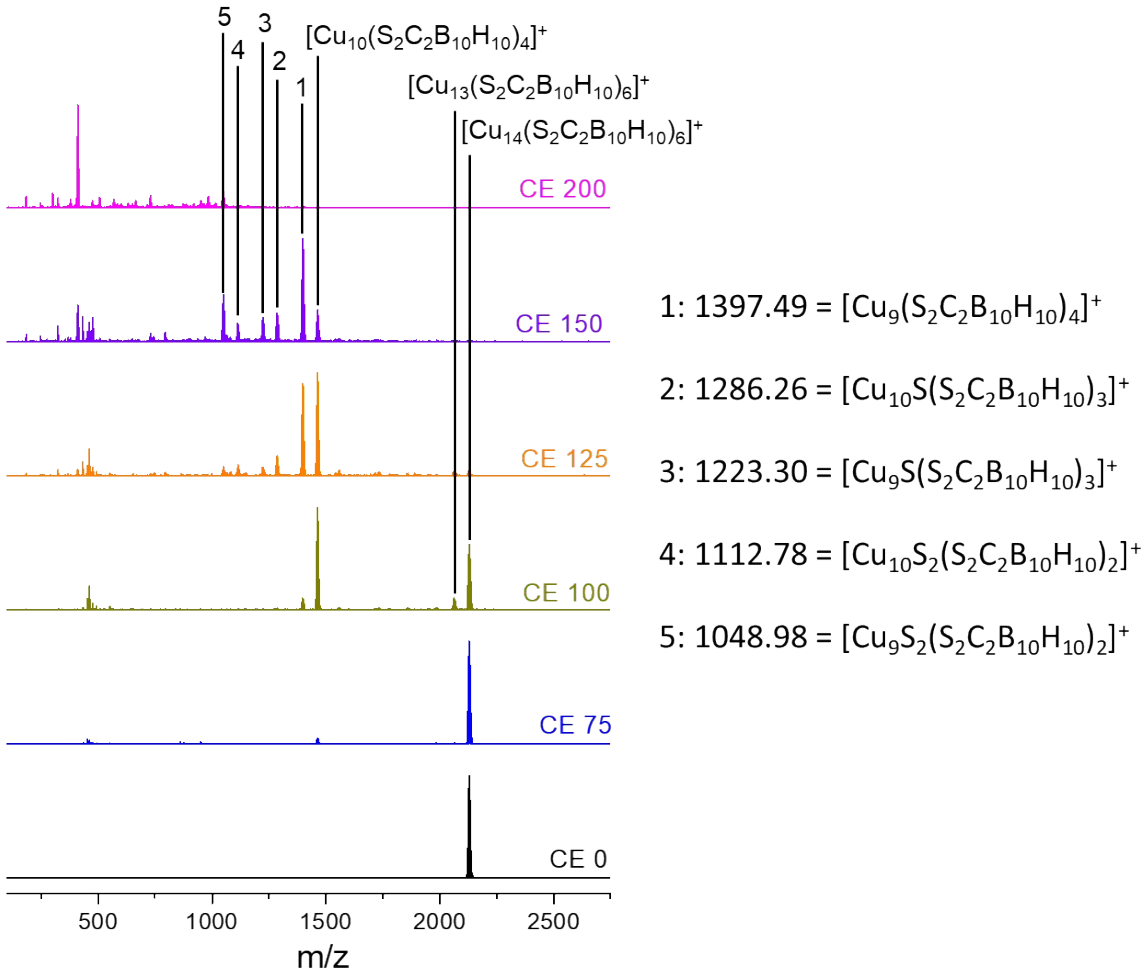

Fig. S1 Collision energy dependent MSMS fragmentation patterns of the selected molecular ion peak (at m/z 2127.74) of the Cu_{14} cluster. Losses of metal kernels and surface ligands from the parent cluster were observed at higher CE.

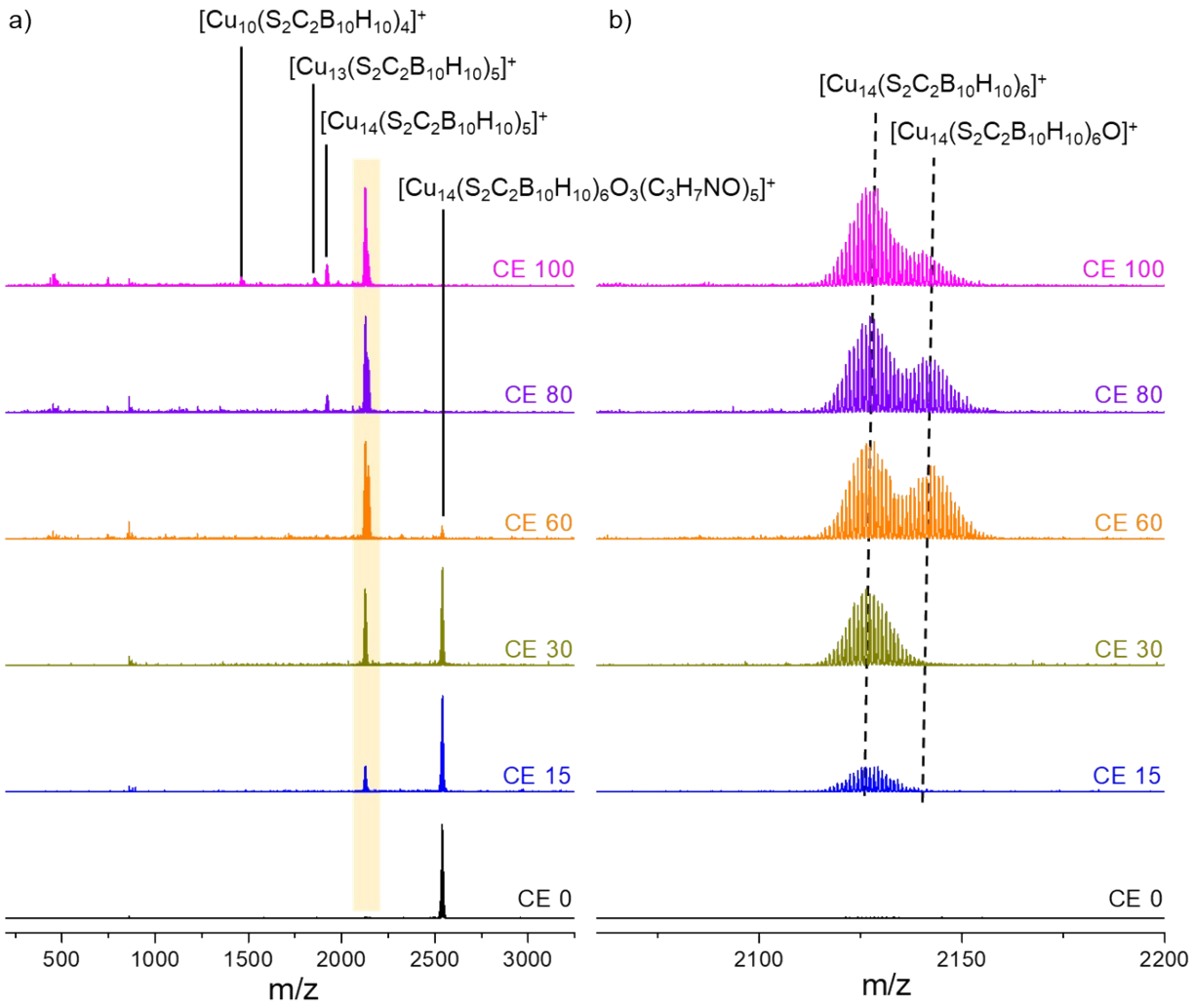

Fig. S2 a) Collision energy dependent MSMS fragmentation patterns of the selected molecular ion peak (at m/z 2540.9) of the Cu_{14}-DMF cluster. Losses of metal kernels and surface ligands were observed from the parent cluster at higher CE. b) Expanded view of the highlighted region.

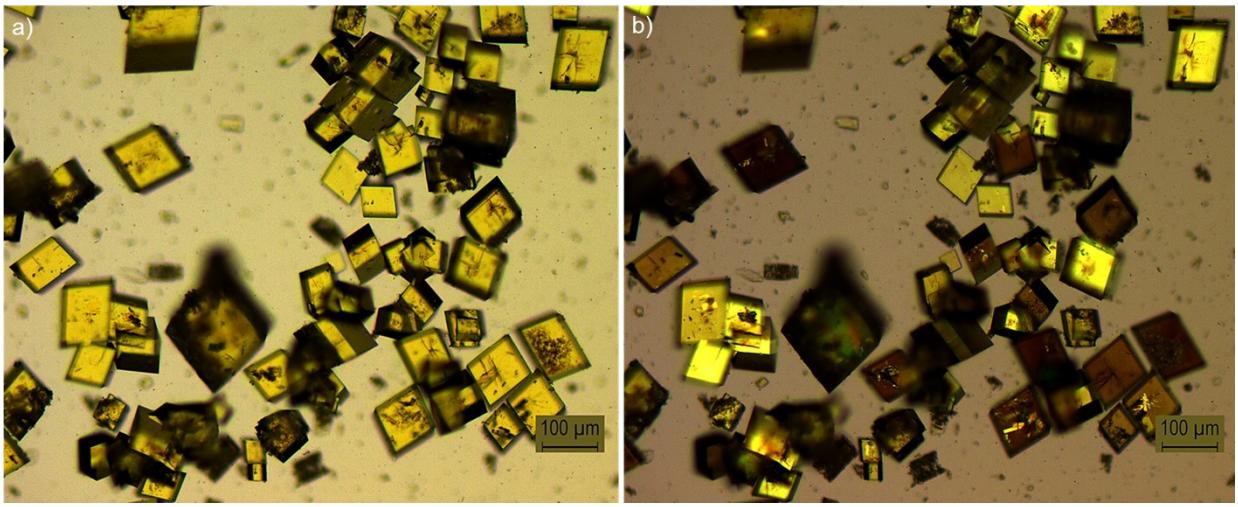

Fig. S3 Optical microscopic images of cuboidal shaped Cu_{14}-DMF crystals a) without polarizer and b) with polarizer.

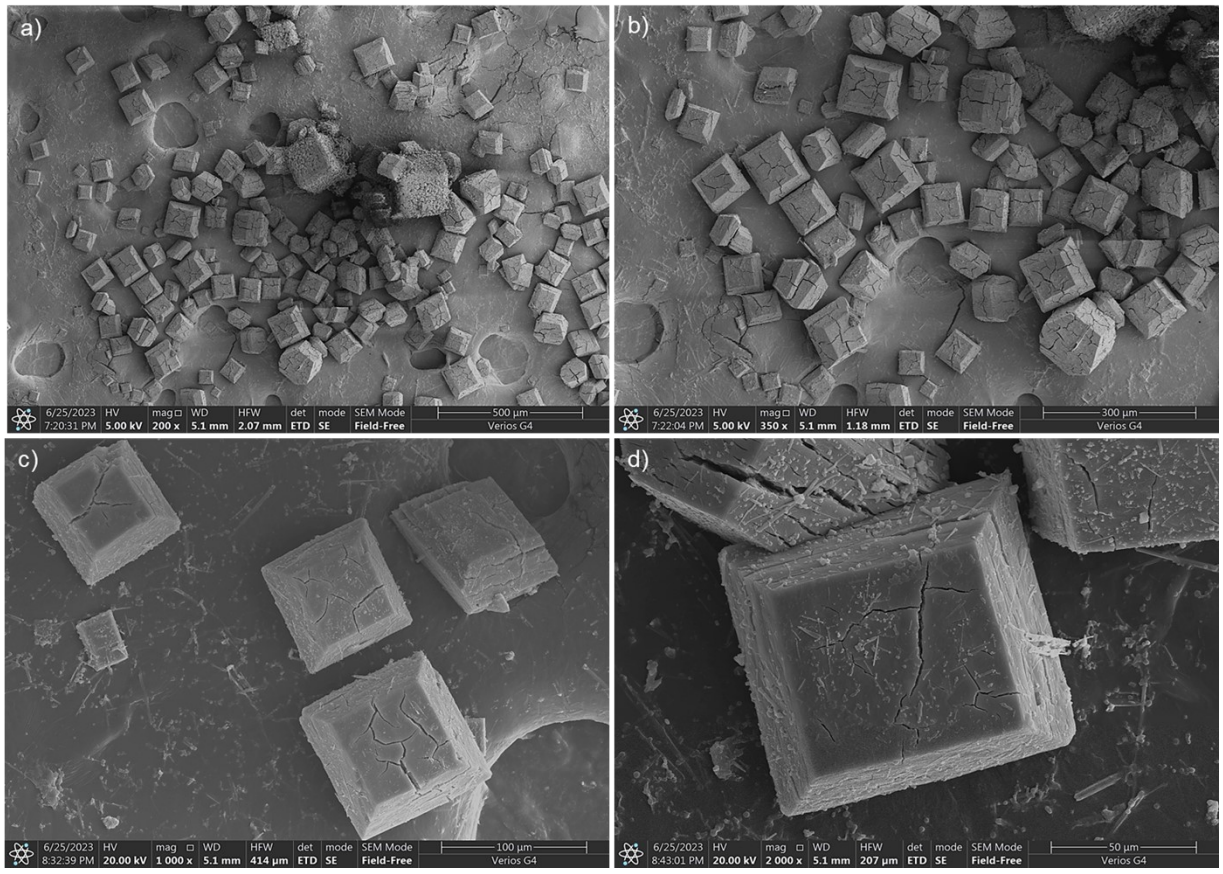

Fig. S4 a-d) Field emission scanning electron micrograph (FESEM) of cuboidal Cu_{14}-DMF crystals at different magnifications. The appearance of the cracks in the crystals is due to the effect of solvent drying.

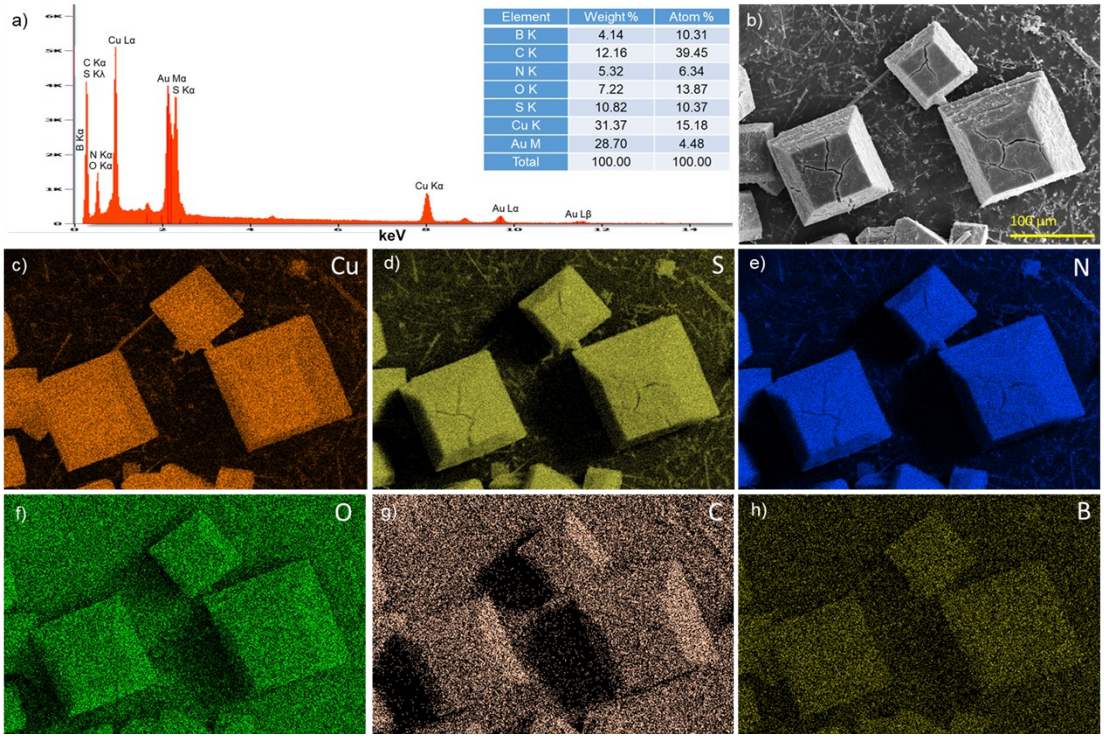

Fig. S5 a) The EDS spectral profile of Cu_{14}-DMF crystals. Inset shows the atomic weight % of various elements present in the crystal. b) FESEM micrograph of the selected crystals used for elemental mapping. c-h) Elemental mapping of the respective elements present in the crystal.

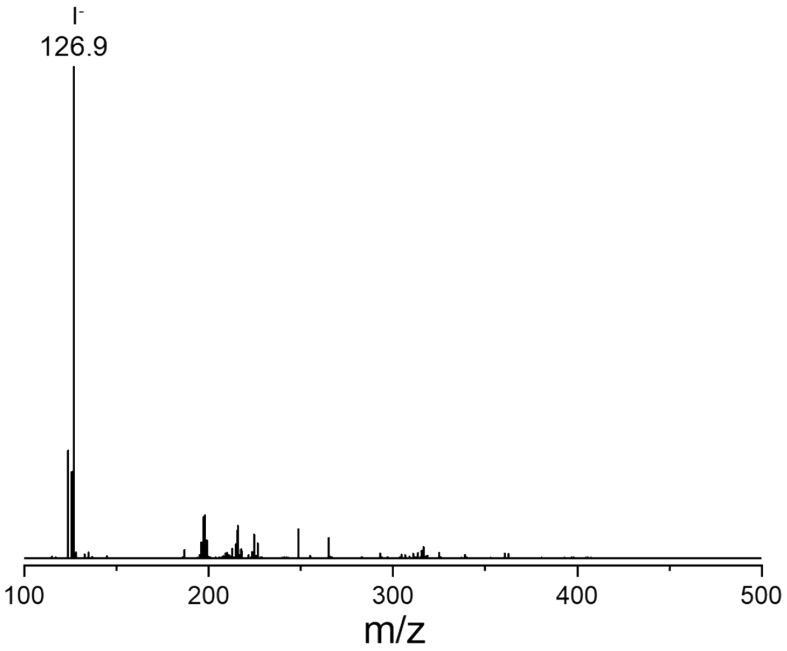

Fig. S6 Negative ion mode ESI mass spectrum of the Cu_{14}-DMF crystals, obtained by dissolving a few crystals in DMF.

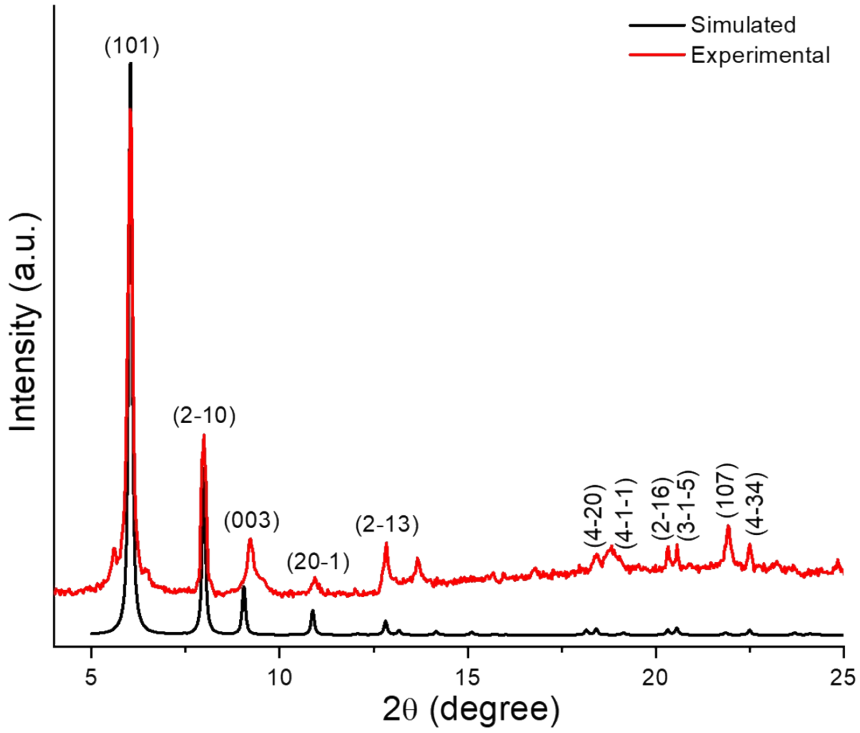

Fig. S7 Comparative PXRD pattern of Cu_{14}-DMF alongside the simulated spectrum derived from single crystal X-ray diffraction.

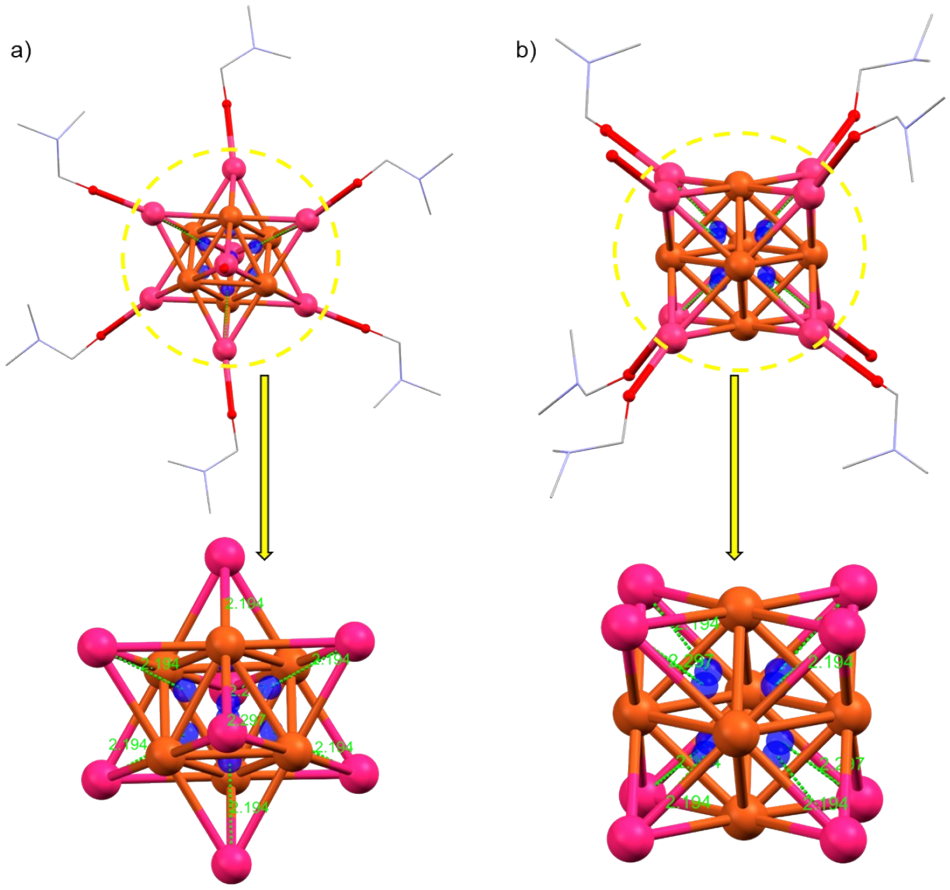

Fig. S8 Structural skeleton of the $[Cu_{14}O_2(DMF)_6]$ skeleton of Cu_{14}-DMF cluster. Distances between the centroids of the Cu_6 octahedral to the outer capped Cu atoms are marked here.

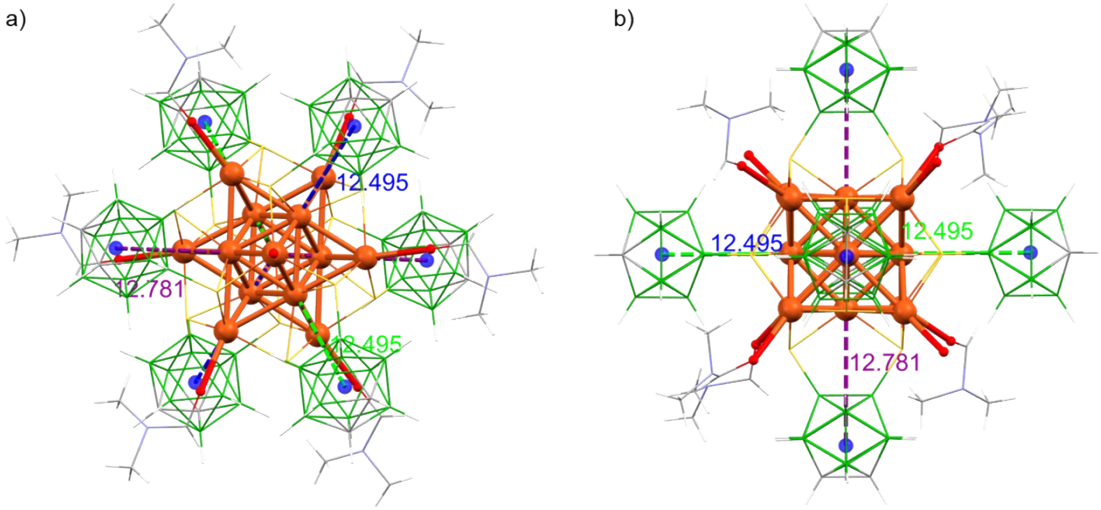

Fig. S9 Distances between the two opposite centroids of the carborane ligands of the Cu_{14}-DMF cluster. a) Top view and b) side view of the cluster.

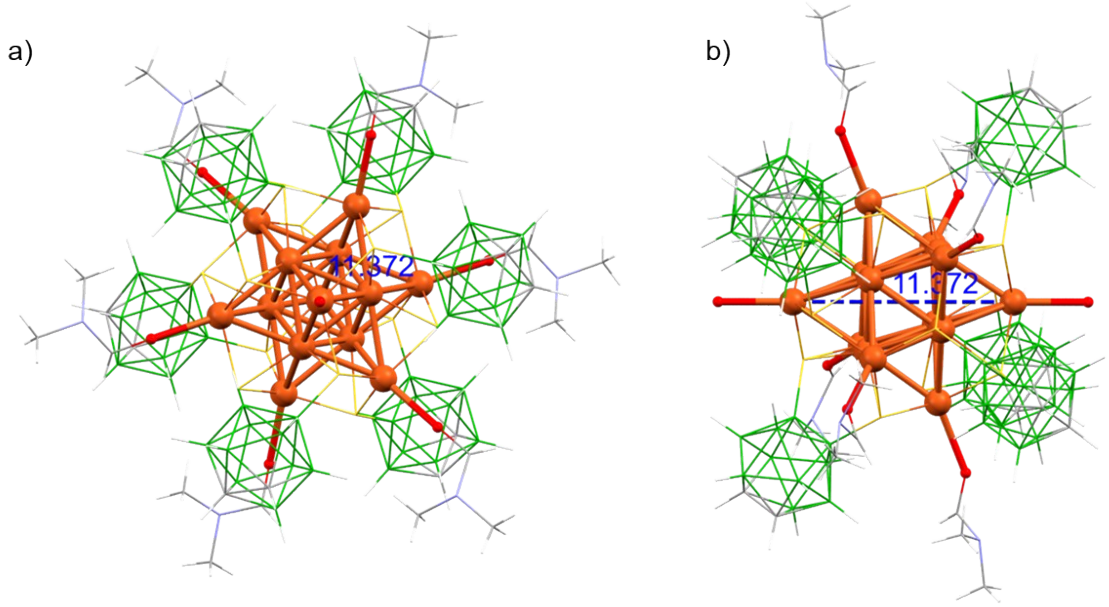

Fig. S10 Interatomic distances between two free oxygens present in the Cu_{14}-DMF cluster. a) Top view and b) side view of the cluster.

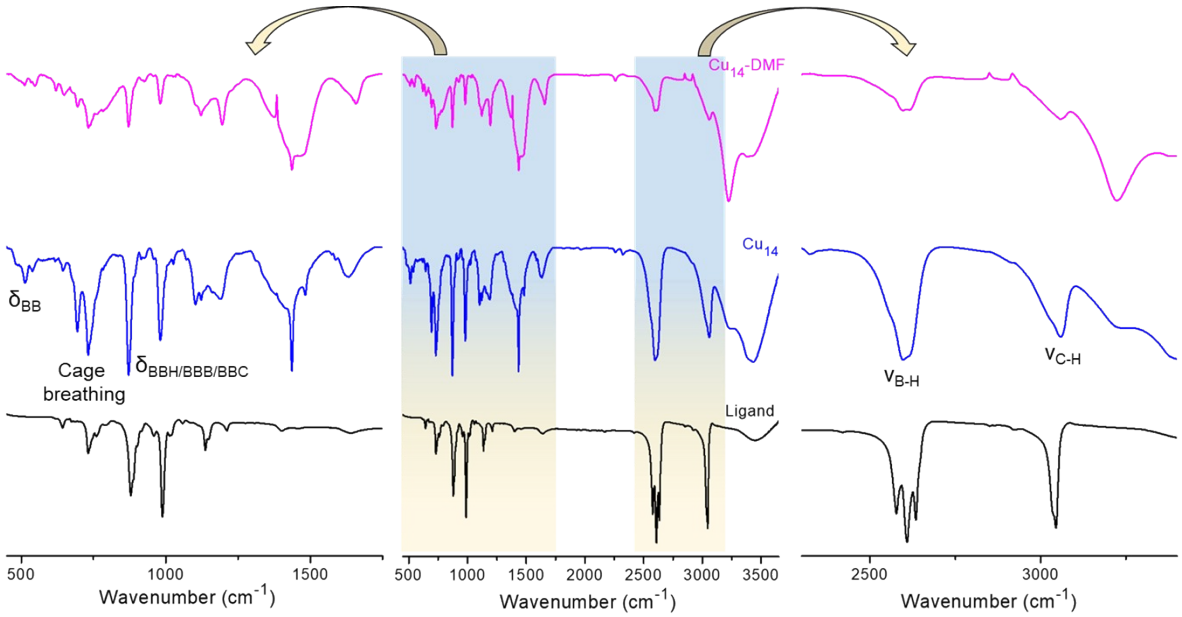

Fig. S11 Comparative IR spectra of *ortho*-carborane 9,12-dithiol ligand, Cu_{14} and Cu_{14}-DMF clusters. Expanded views of the highlighted regions with respective assignments are shown.

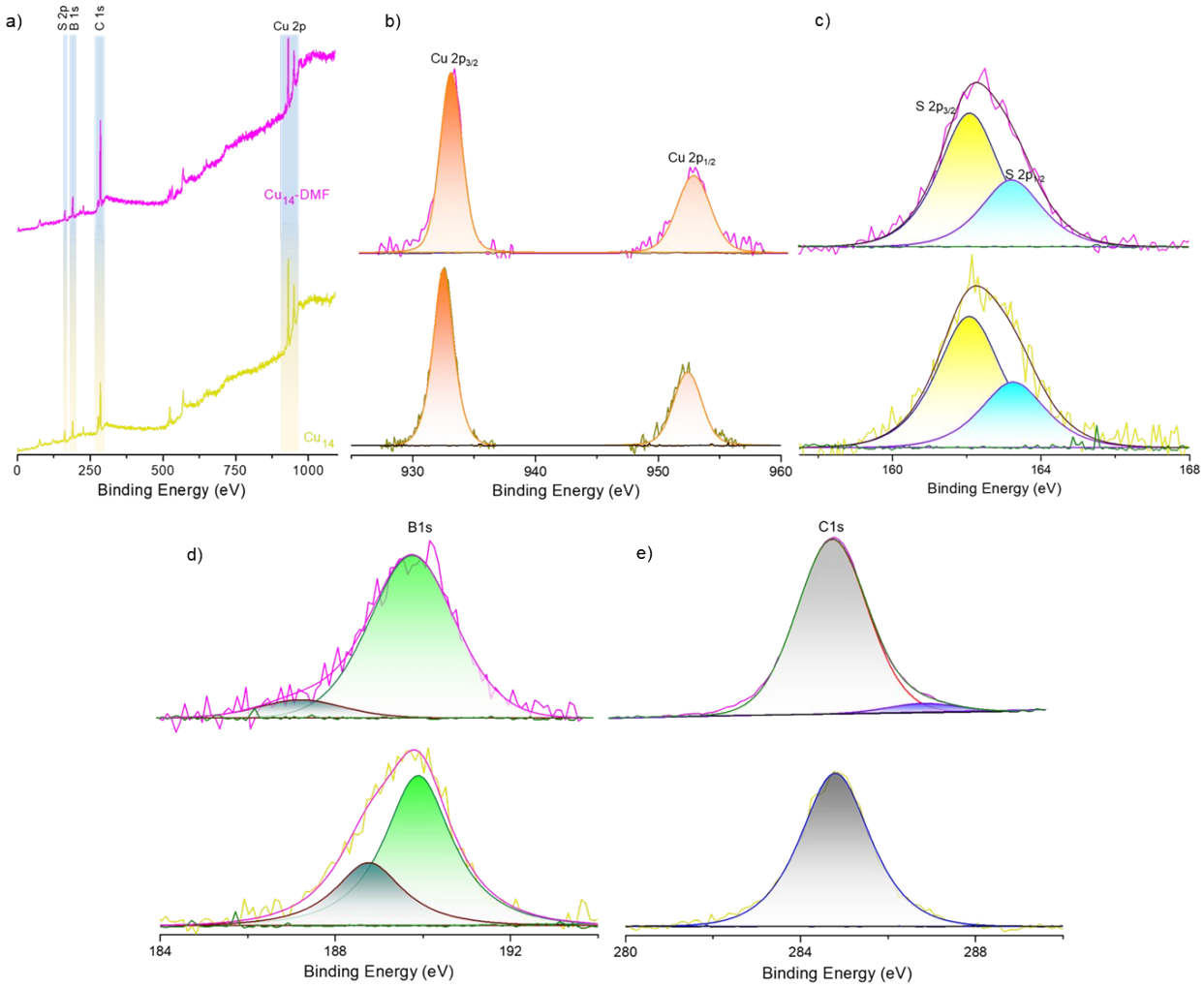

Fig. S12 Comparative XPS spectra of Cu_{14} and Cu_{14}-DMF clusters. a) Survey spectra and selected spectral fittings of b) Cu 2p, c) S 2p, d) B 1s, and e) C 1s regions. Color code of the spectrum: brown line: Cu_{14} and pink line: Cu_{14}-DMF.

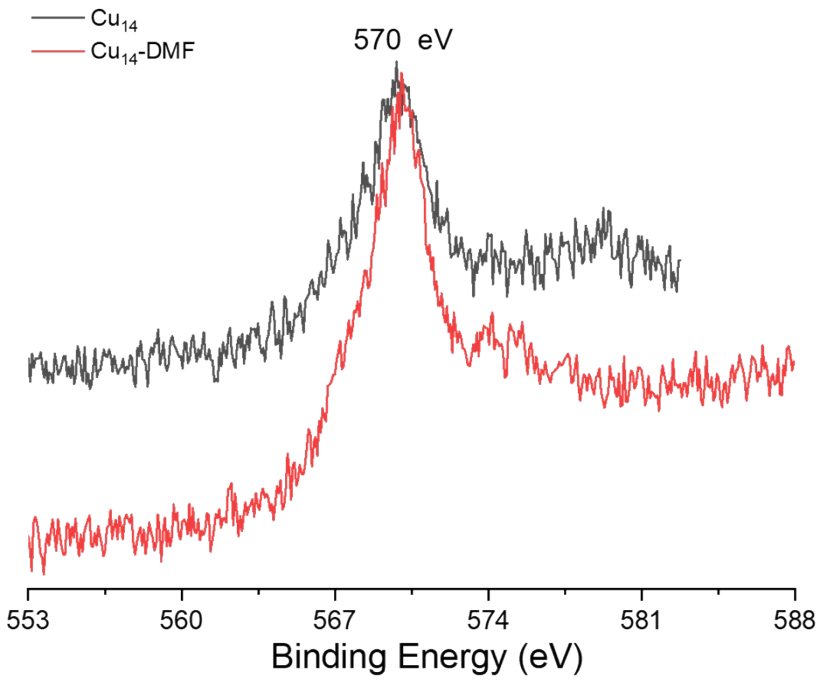

Fig. S13 Comparative Cu LMM Auger spectra of Cu_{14} and Cu_{14}-DMF clusters.

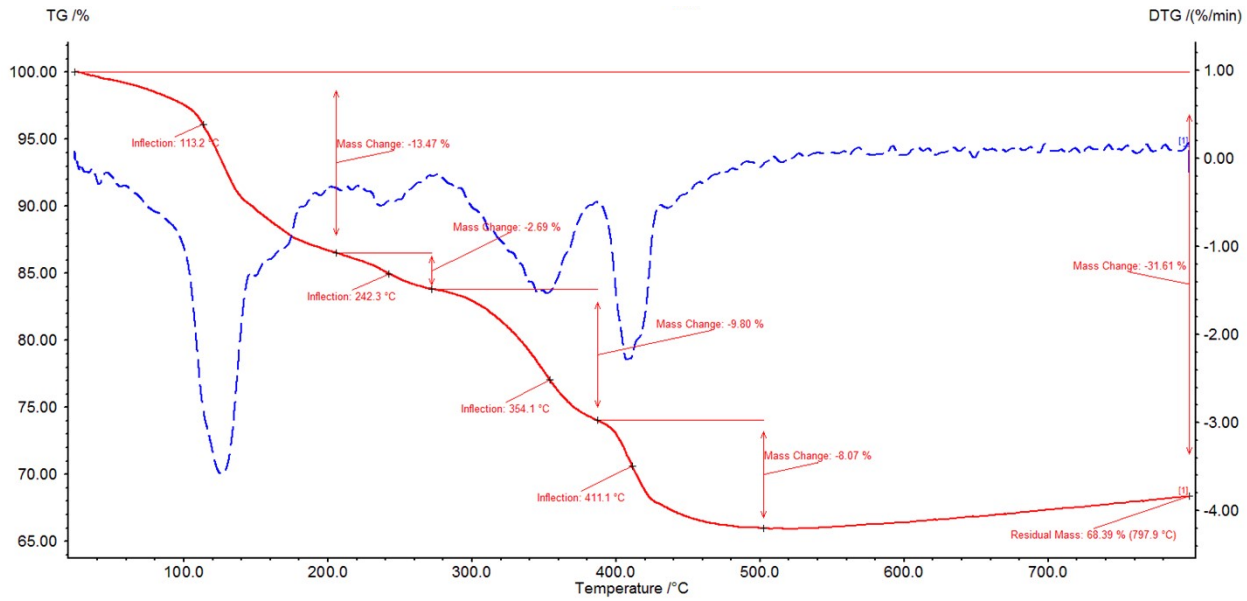

Fig. S14 Thermogravimetric (TG) and differential TG analysis of Cu_{14} cluster under nitrogen atmosphere at a flow rate of 20 ml/min. The heating gradient was 10 K/ min.

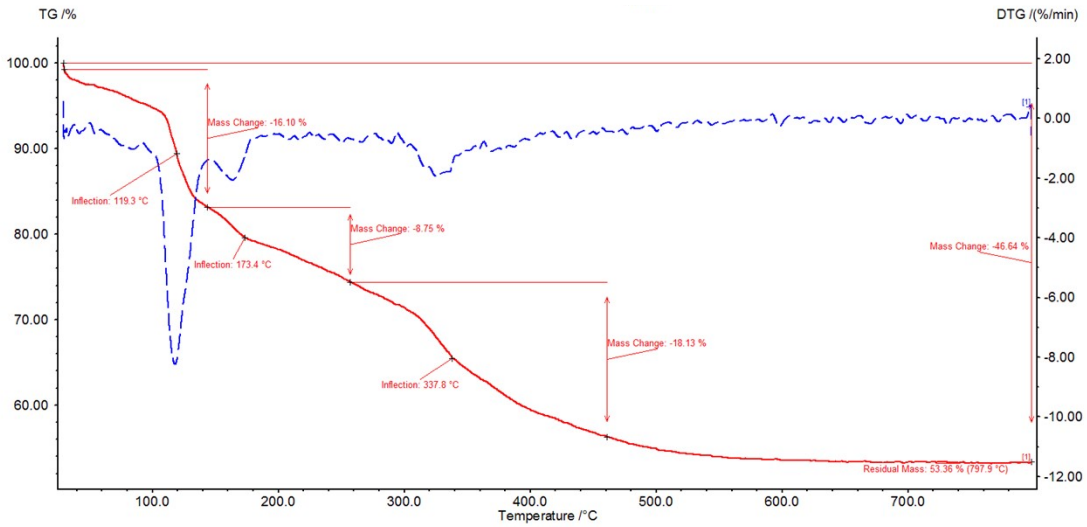

Fig. S15 Thermogravimetric (TG) and differential TG analysis of Cu_{14}-DMF cluster under nitrogen atmosphere at a flow rate of 20 ml/min. The heating gradient was 10 K/ min.

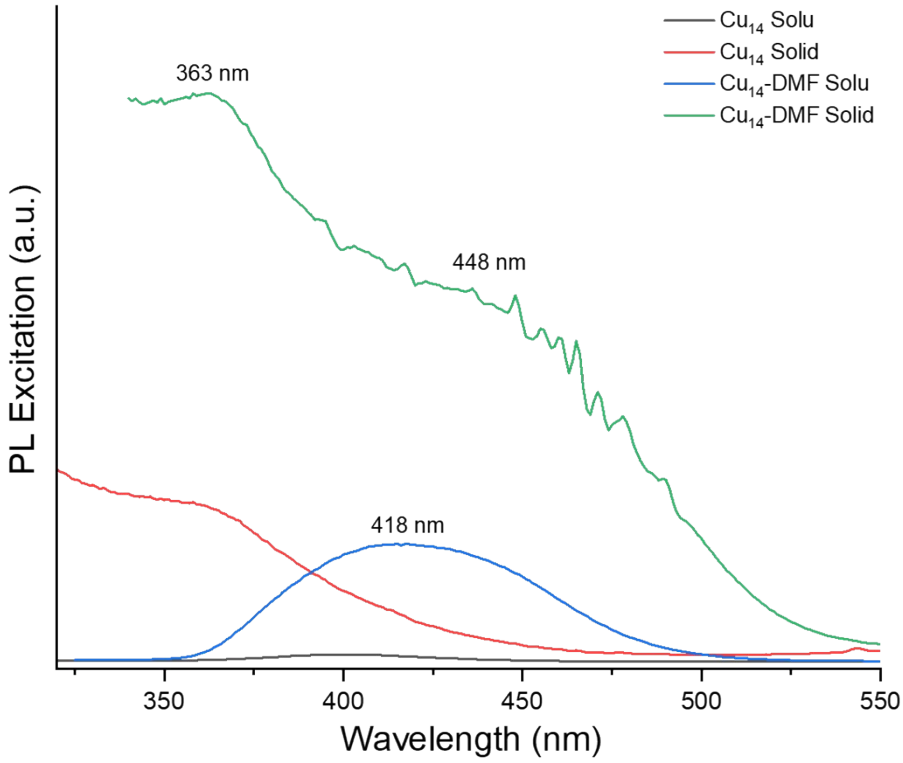

Fig. S16 Photoluminescence excitation spectra of Cu_{14} and Cu_{14}-DMF clusters in their respective states.

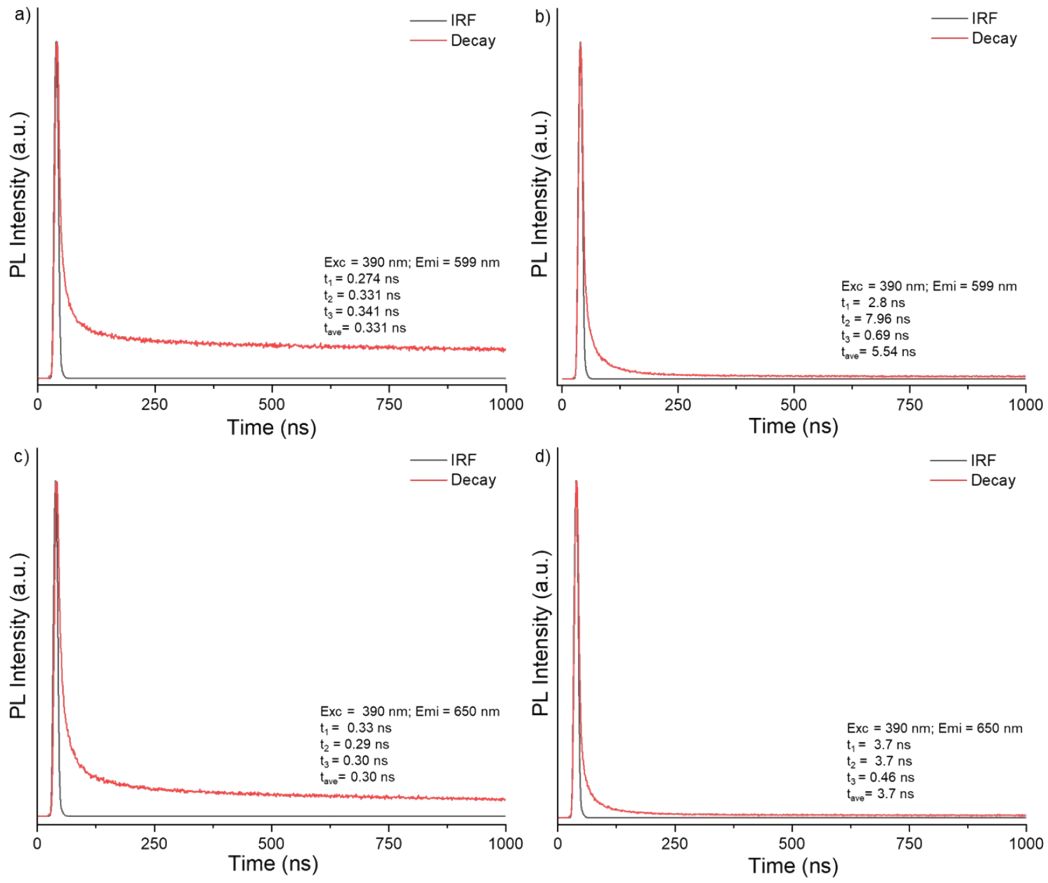

Fig. S17 Luminescence decay profiles and respective decay times of as prepared Cu_{14} cluster in a) DCM solution and b) solid state and Cu_{14}-DMF cluster in c) DMF solution and d) solid state.

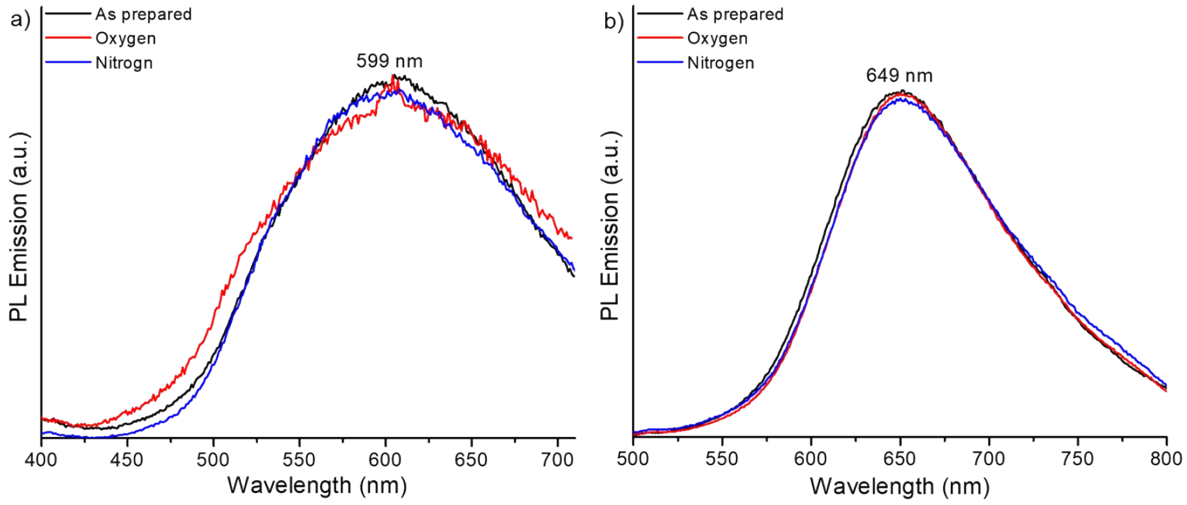

Fig. S18 PL emission spectra of a) Cu_{14} and b) Cu_{14}-DMF in their respective solutions showed no change in their emission intensity upon oxygen exposure.

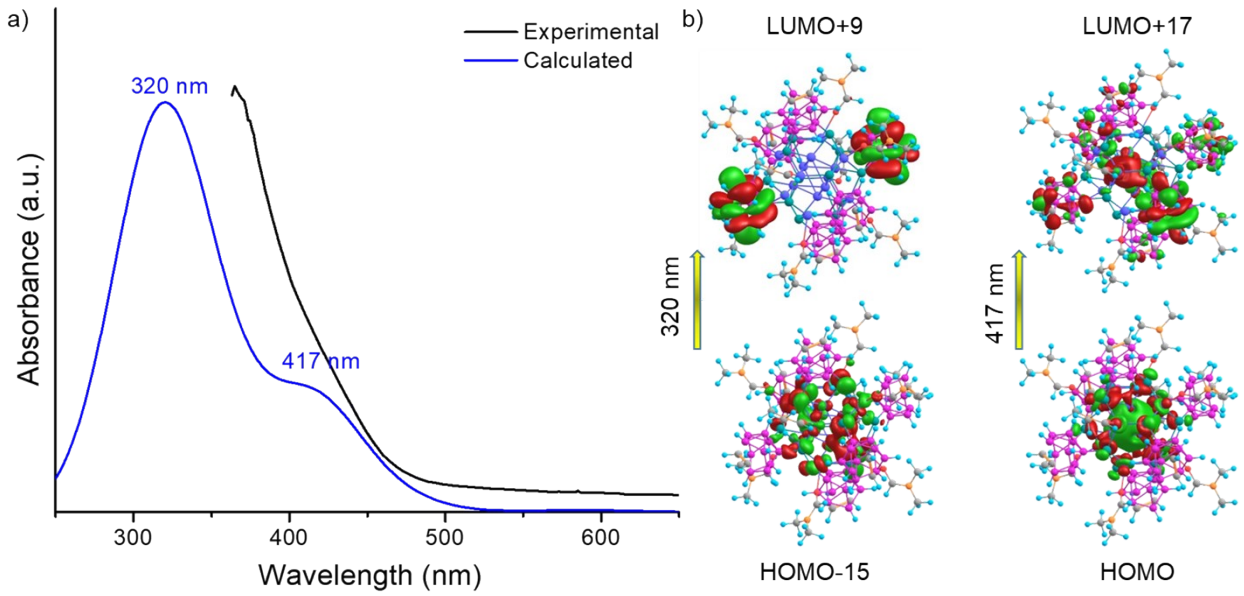

Fig. S19 a) Comparative UV-vis absorption spectrum of Cu_{14}-DMF cluster shows the matching of the experimental and simulated spectrum. b) Molecular orbitals associated with the respective absorption features.

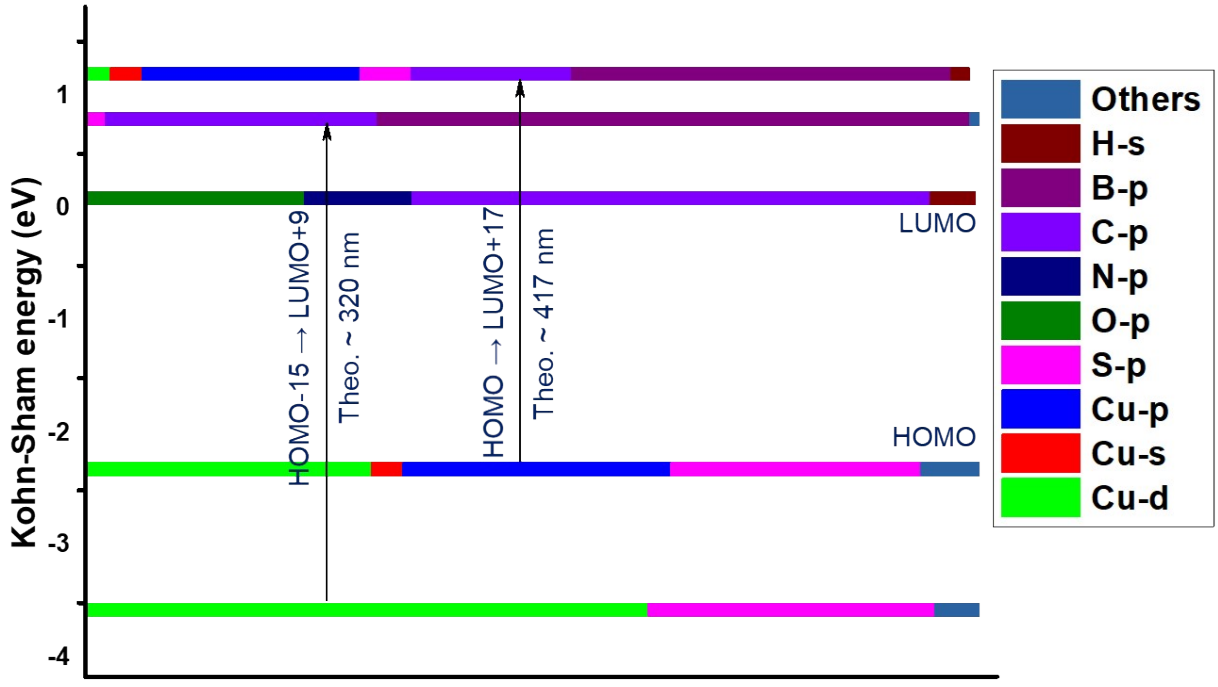

Fig. S20 Kohn-Sham electronic energy level diagram for Cu_{14}-DMF cluster. Electronic transitions of the optical absorption features are marked here.

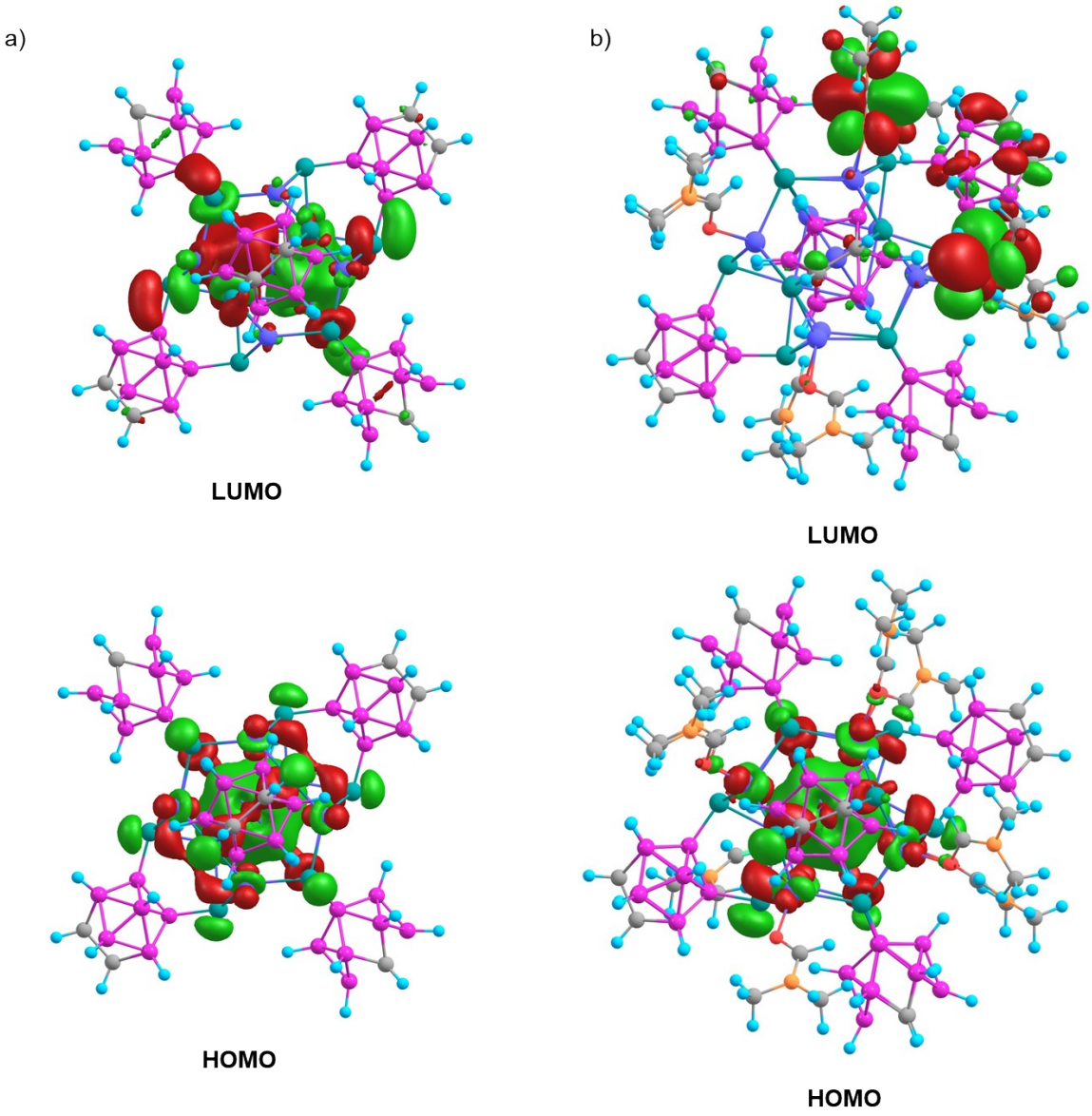

Fig. S21 Frontier molecular orbitals of a) Cu_{14} and b) Cu_{14}-DMF clusters.

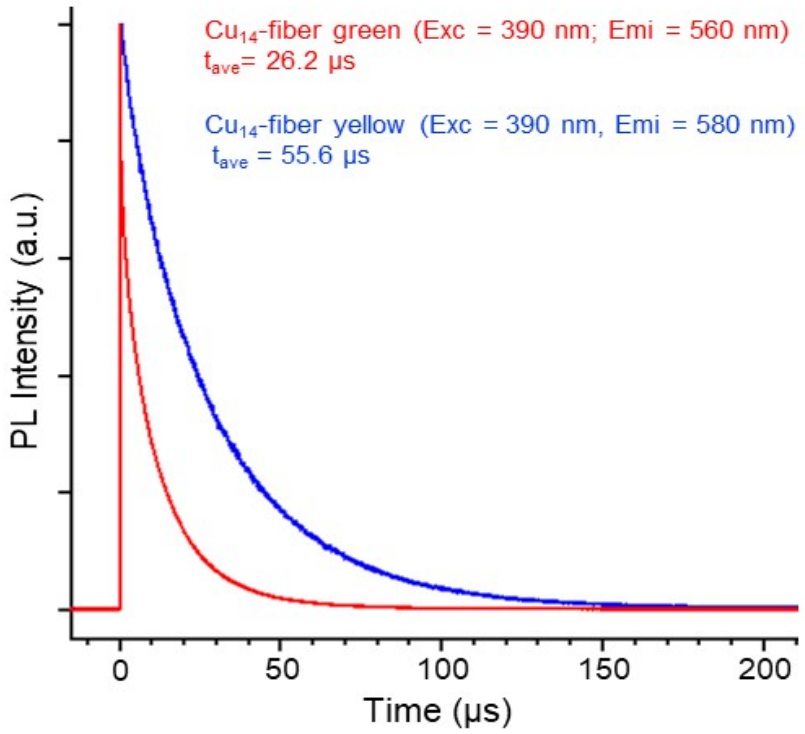

Fig. S22 Luminescence decay profiles of green and yellow emitting Cu_{14}-fibers at room temperature.

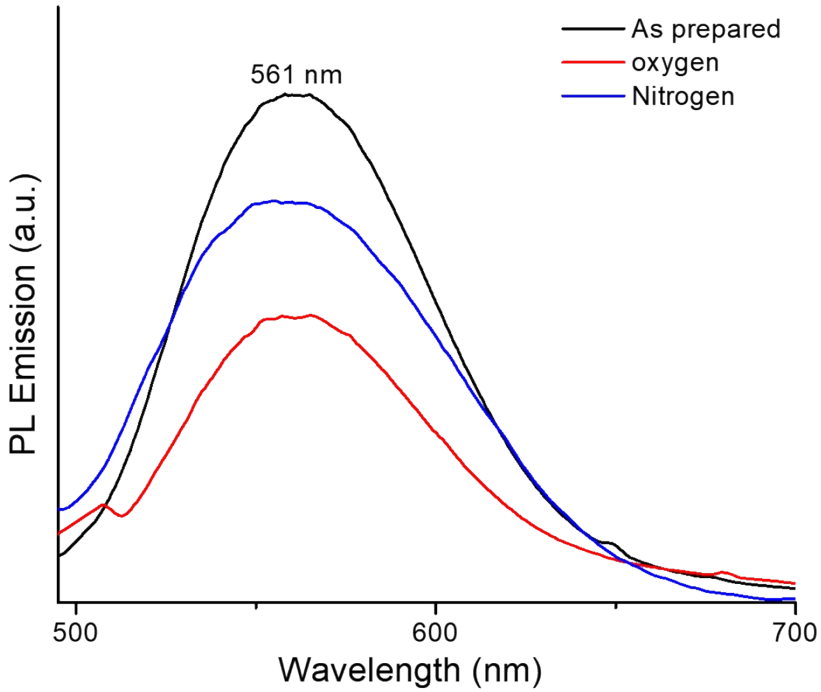

Fig. S23 Comparative PL studies were conducted on green emitting Cu_{14}-fibers, both pre- and post-exposure to oxygen gas. Subsequently, nitrogen was introduced after the oxygen exposure. Excitation was at 400 nm.

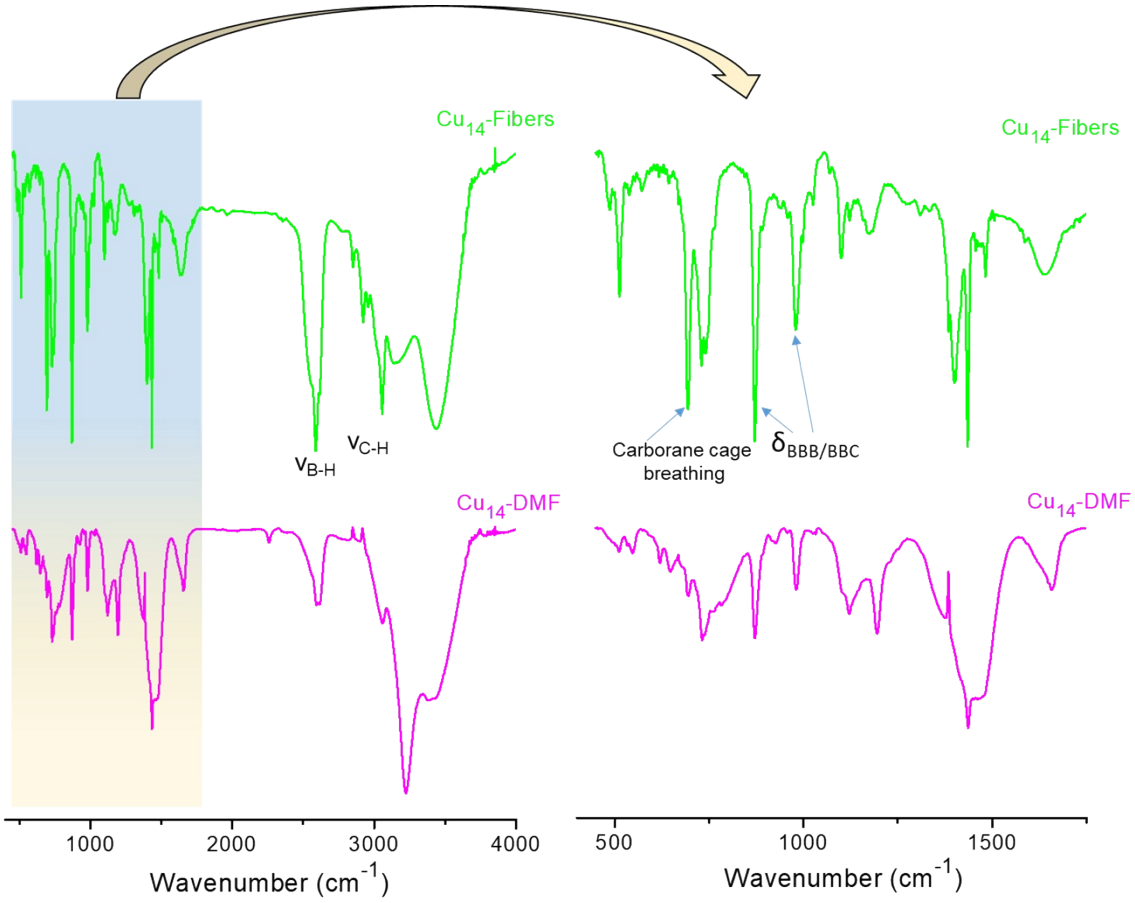

Fig. S24 Comparative IR spectra of Cu_{14}-DMF cluster and Cu_{14}-fibers.

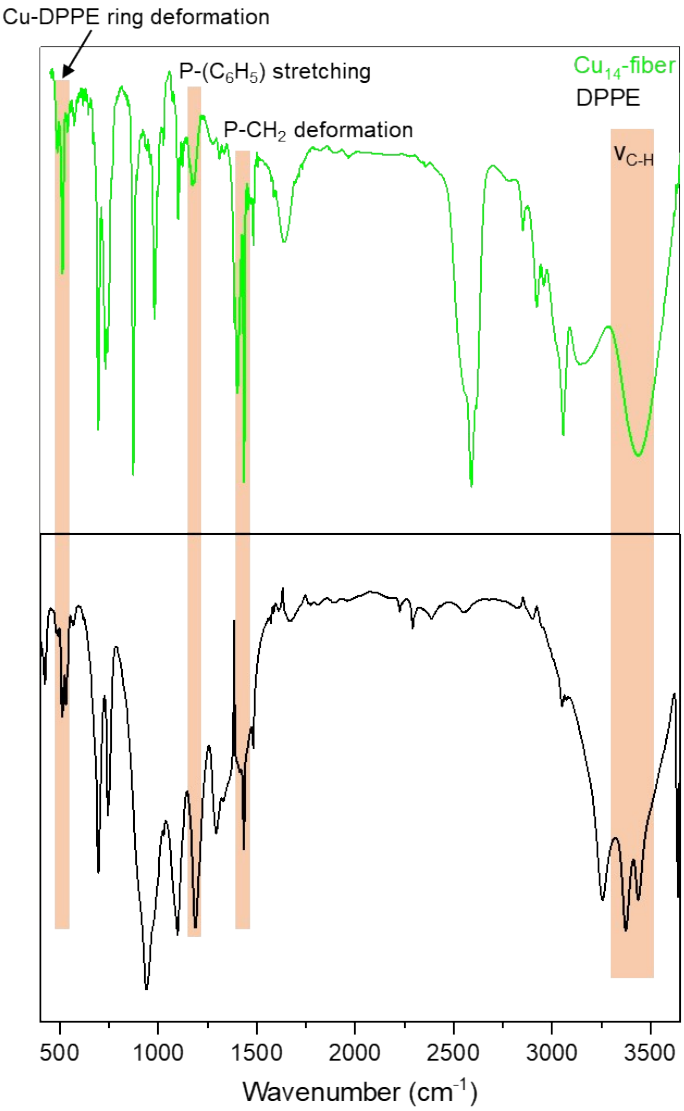

Fig. S25 Comparative IR spectra of free DPPE and Cu_{14}-fibers. Minor variations in the highlighted peak positions indicate the binding of DPPE to the cluster.

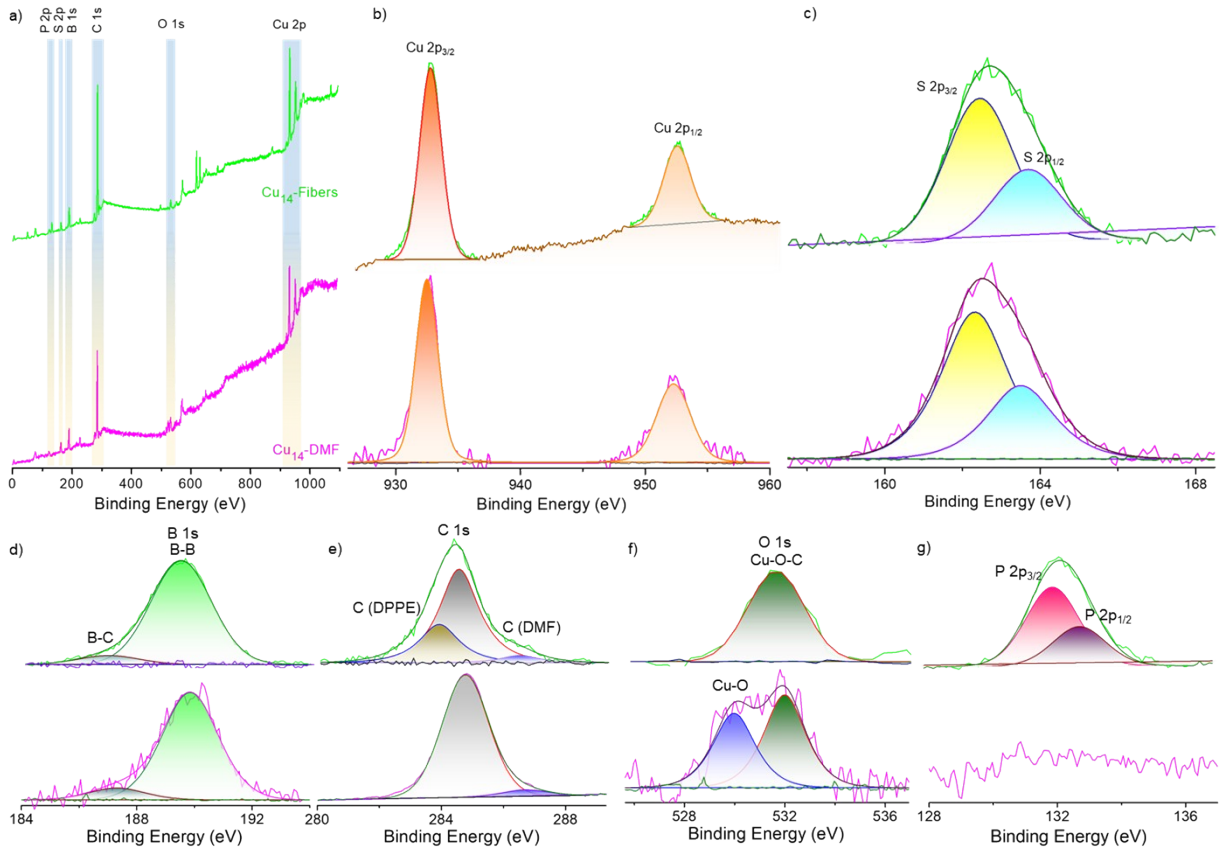

Fig. S26 Comparative XPS a) survey spectra of Cu_{14}-DMF and Cu_{14}-fibers. Selected area spectral fittings of b) Cu 2p, c) S 2p, d) B 1s, e) C 1s, f) O 1s, g) P 2p regions. Color code: green line = Cu_{14}-fibers, pink = Cu_{14}-DMF.

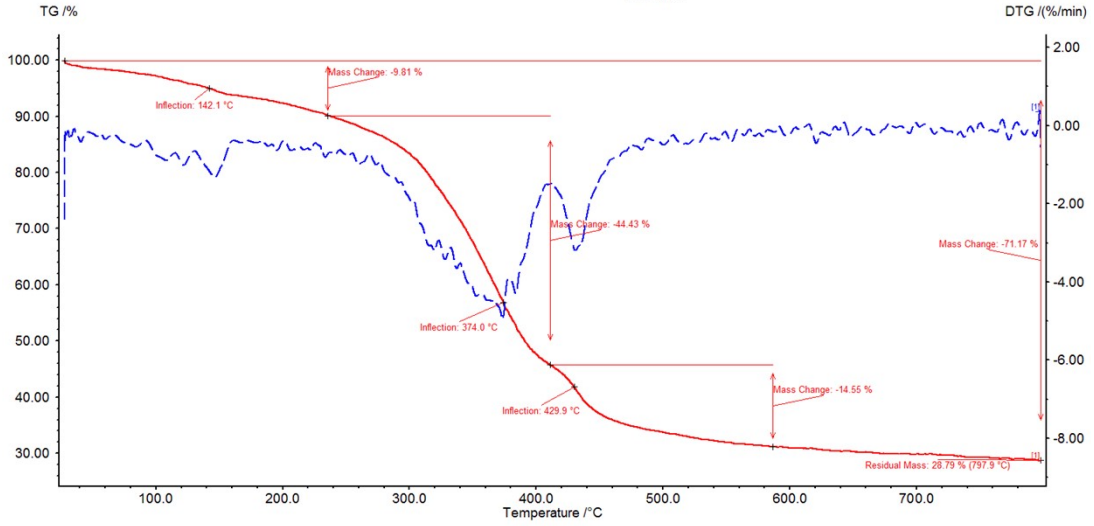

Fig. S27 Thermogravimetric (TG) and differential TG analysis of Cu_{14}-fibers under nitrogen atmosphere at a flow rate of 20 ml/min. The heating rate was 10 K/ min.

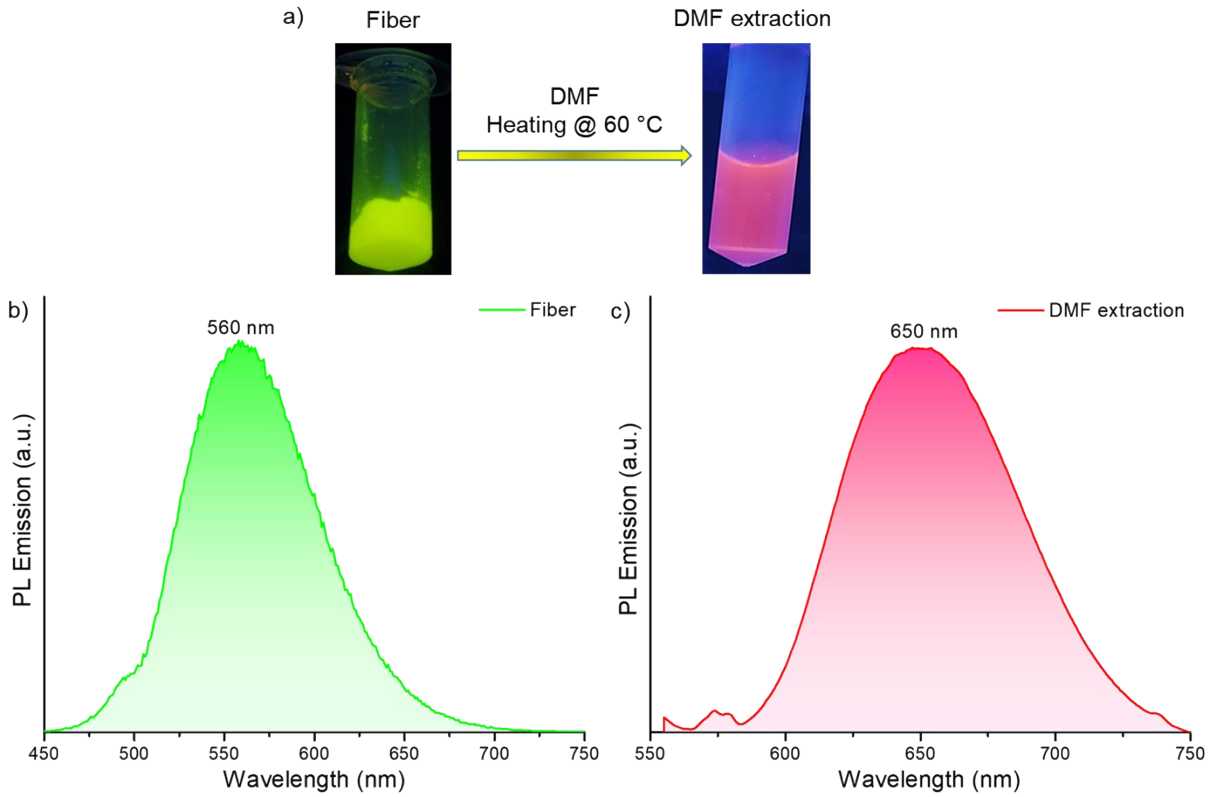

Fig. S28 a) Photographs of the Cu_{14}-fibers under UV light and after its extraction in DMF. PL emission profiles of the b) fiber, and c) the extracted DMF solution.

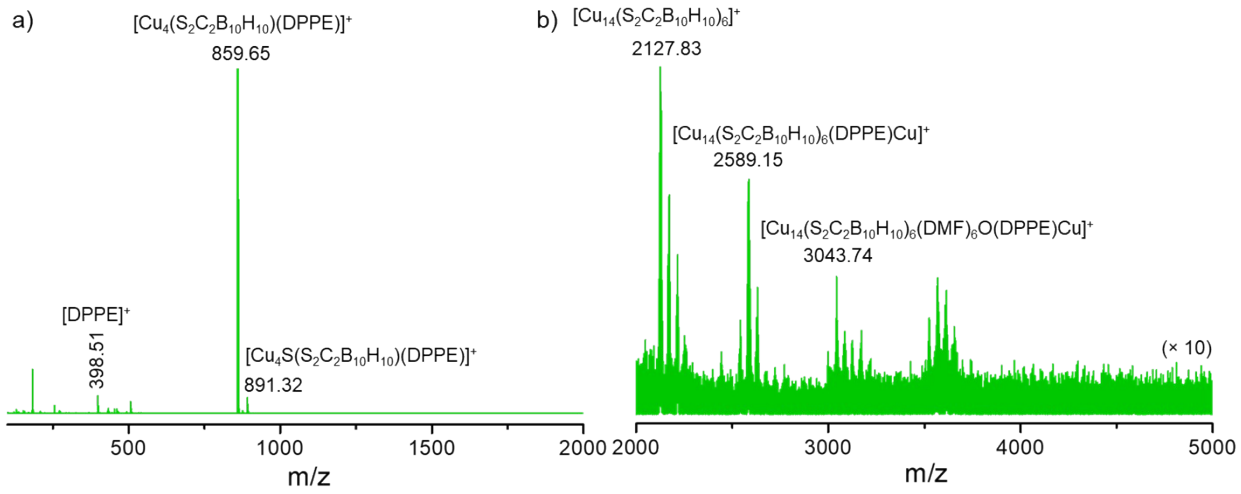

Fig. S29 Positive ion mode ESI-MS spectrum of Cu_{14}-fibers after dissolving them in DMF. a) Mass range of m/z 100-2000 and b) expanded view of the spectrum in the mass range of m/z 2000-5000. Peaks of interest are marked here.

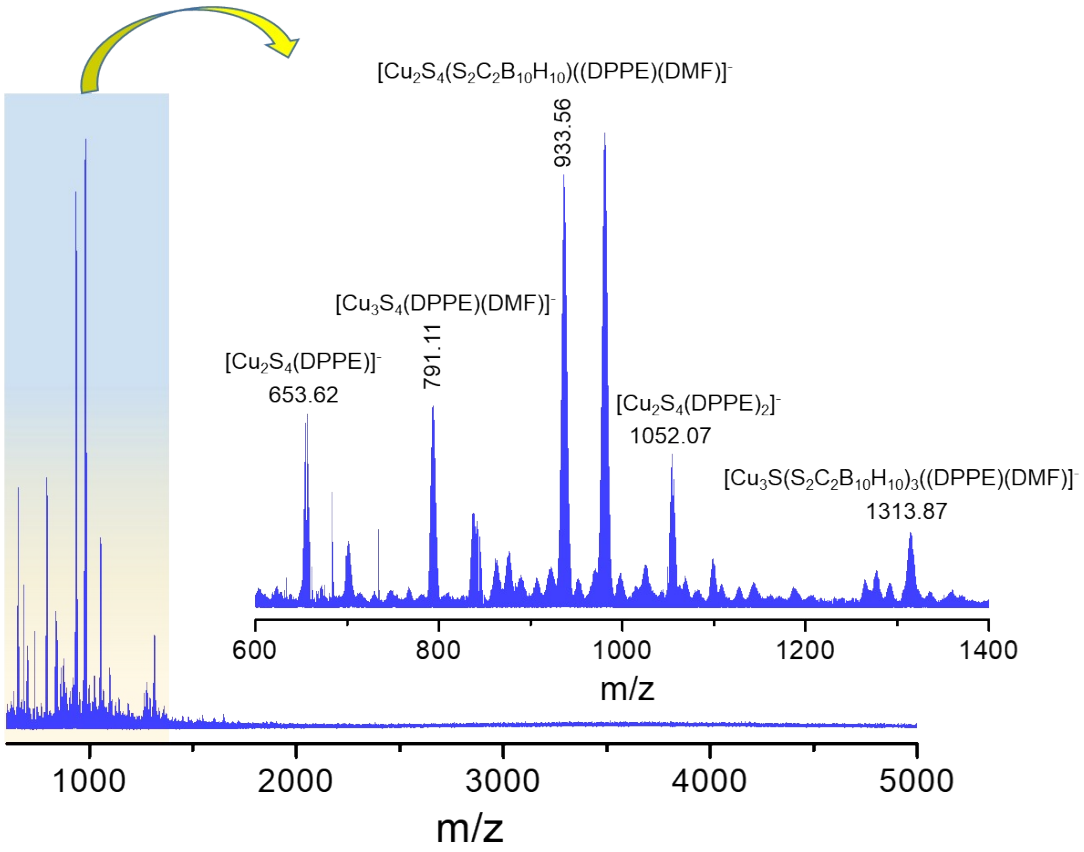

Fig. S30 Full range negative ion mode ESI-MS spectrum of Cu_{14}-fibers after dissolving them in DMF. Inset shows an expanded view of the spectrum along with the respective peaks are marked here. Appearance of DPPE attached Cu peaks indicate the 1D assembly of DPPE linkers with the clusters.

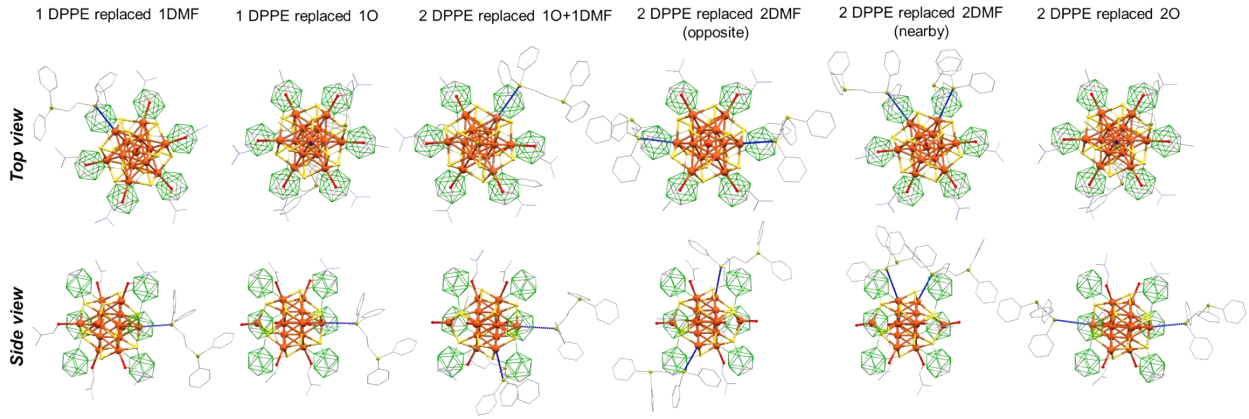

Fig. S31 Optimized structural models of most probable bindings of DPPE linkers with the Cu_{14}-DMF cluster. Hydrogen atoms are removed for clarity. Color codes: orange = copper, yellow = sulfur, green = boron, grey = carbon, red = oxygen and brown = phosphorus.

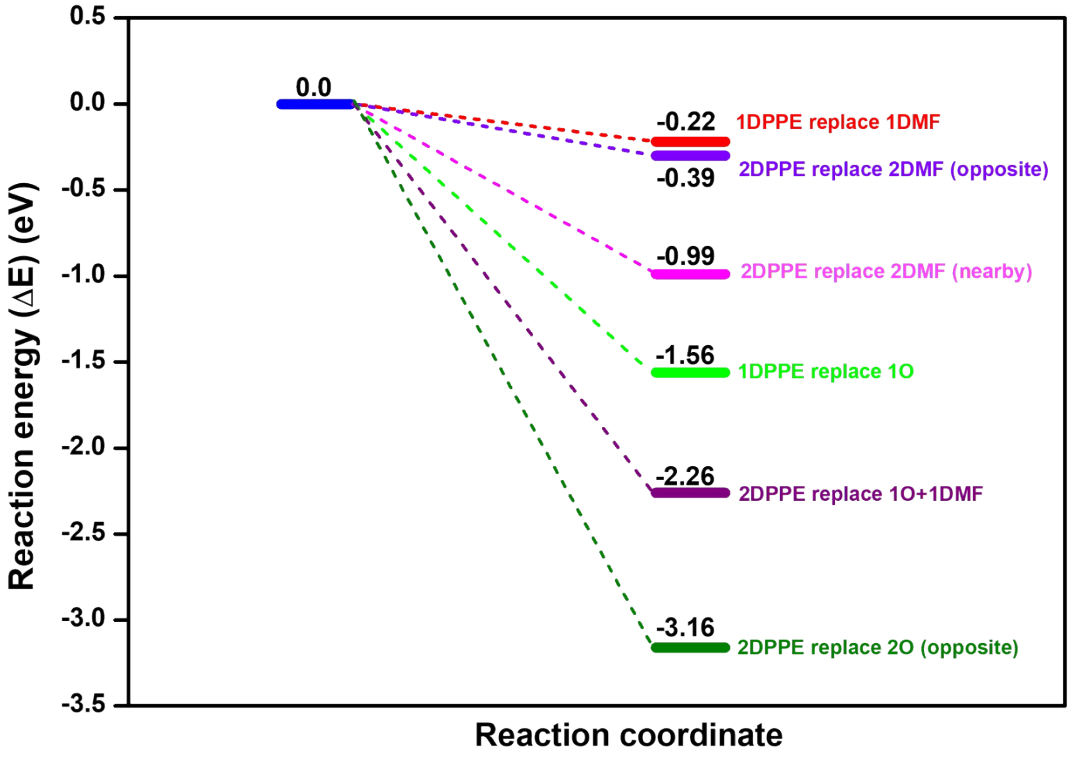

Fig. S32 A comparative energy profile of the probable binding of DPPE linkers at various positions of the Cu_{14}-DMF cluster.

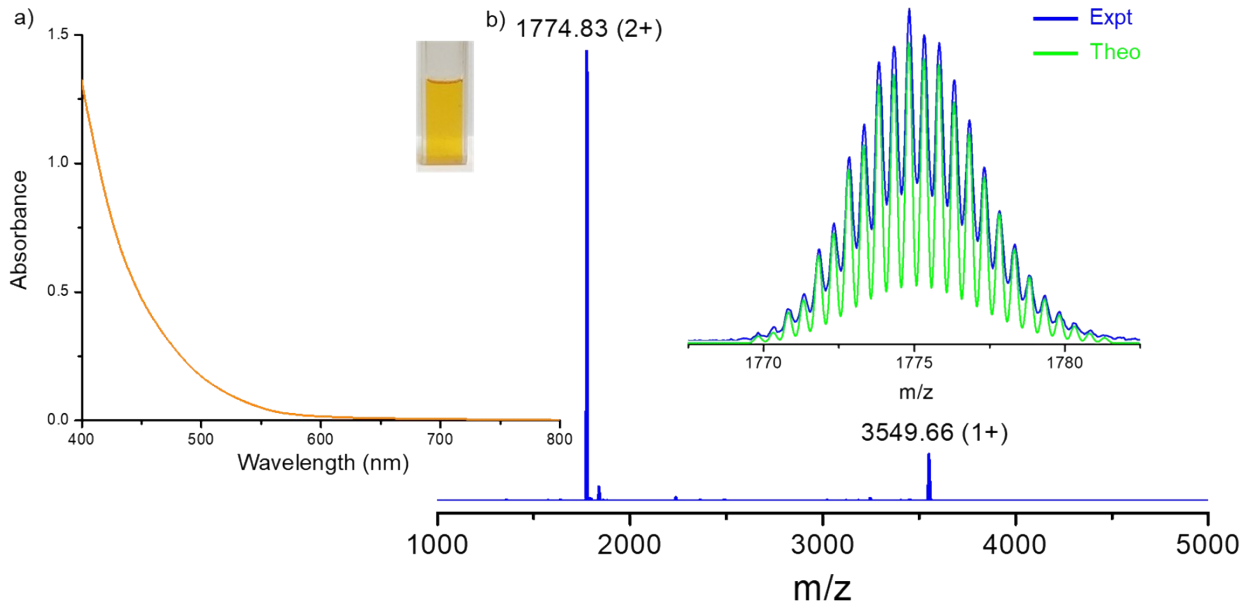

Fig. S33 a) UV-vis absorption spectrum of $[Cu_{18}(DPPE)_6H_{16}]$ nanocluster. Inset shows the photographic image of the cluster in DCM. b) Full range mass spectrum of the Cu_{18} cluster in positive ion mode shows the presence of di- (at m/z 1774.83) and mono- cationic (at m/z 3549.66) species for the cluster. Inset shows

the exact matching of the isotopic distributions of the experimental and theoretical spectra for the 2+ charge state species.

References

1. A. Jana, M. Jash, W. A. Dar, J. Roy, P. Chakraborty, G. Paramasivam, S. Lebedkin, K. Kirakci, S. Manna, S. Antharjanam, J. Machacek, M. Kucerakova, S. Ghosh, K. Lang, M. M. Kappes, T. Base and T. Pradeep, *Chem. Sci.*, 2023, **14**, 1613–1626.
2. Frisch, M. J.; Trucks, G. W.; Schlegel, H. B.; Scuseria, G. E.; Robb, M. A.; Cheeseman, J. R.; Scalmani, G.; Barone, V.; Mennucci, B.; Petersson, G. A. et al. Gaussian 09, Revision B.01; Gaussian Inc.: Wallingford, CT, **2009**.
3. A. D. Becke, *Phys. Rev. A: At., Mol., Opt. Phys.,* 1988, **38**, 3098–3100.
4. A. D. Becke, *J. Chem. Phys.*, 1993, **98**, 1372–1377.
5. W. J. Hehre, R. Ditchfield and J. A. Pople, *J. Chem. Phys.*, 1972, **56**, 2257–2261.
6. P. C. Hariharan and J. A. Pople, *Theor. Chim. Acta*, 1973, **28**, 213–222.
7. T. Lu and F. Chen, *J. Comput. Chem.*, 2012, **33**, 580–592.